



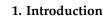
Article Study on the Thermodynamic Properties of Thin Film of FCC Interstitial Alloy AuSi at Zero Pressure Using the Statistical Moment Method

Nguyen Thi Hoa ^{1,*}, Nguyen Quang Hoc ² and Hua Xuan Dat ²

- ¹ Department of Physics, Faculty of Basic Sciences, University of Transport and Communications, 3 Cau Giay, Dong Da, Hanoi 11500, Vietnam
- ² Department of Theoretical Physics, Faculty of Physics, Hanoi National University of Education, 136 Xuan Thuy, Cau Giay, Hanoi 11300, Vietnam
- Correspondence: nthoaly@utc.edu.vn

Abstract: We built a model and proposed a theory about the thermodynamic properties of facecentered cubic (FCC) binary interstitial alloy's thin films based on the statistical moment method and performed numerical calculations for AuSi (gold silicide). First, the statistical moment method (SMM) calculations for the thermodynamic properties of Au are compared with reported experiments and calculations that show a good agreement between the calculations in this paper and earlier studies. Additionally, the SMM calculations for thermodynamic properties of AuSi alloy films are performed, which show that the thermal expansion coefficient, the specific heat at constant volume, and the specific heat at constant pressure increases, while the isothermal elastic modulus decreases with increasing temperature and increasing interstitial atom concentration. Furthermore, when the number of layers reaches 100, the thermodynamic properties of the film are similar to those of the bulk material. The achieved theoretical results for AuSi films are novel and can be useful in designing future experiments.

Keywords: binary interstitial alloy; thin film; thermodynamic properties; statistical moment method



Among recent theoretical approaches regarding the thermodynamic properties of solid phases, molecular dynamics simulation [1] and density functional theory [2] are certainly the most effective approaches even though they are somewhat time consuming. In contrast, for simple non-magnetic metals, a model using an empirical potential may be effective to determine the thermodynamic parameters. The self-consistent phonon theory in the reduced second-order [3], self-consistent statistical method [4] and the statistical moment method (SMM) [5] can be steadily used to derive thermodynamic and transport properties of a crystal or a film. The SMM is a modern method in quantum statistical mechanics that considers the anharmonicity effect of lattice vibrations, the correlation effect, and the effects of pressure, temperature and atomic concentration. The thermodynamic, elastic, melting and structural phase transition quantities calculated using the SMM have the form of analytic expressions and are easy for numerical calculations. In many cases, the results calculated using the SMM agree better with the experimental data than the results obtained with other methods. The SMM has been applied to study elastic moduli and elastic constants of FCC interstitial alloy AuCuSi under pressure [6], thermodynamic and elastic properties of BCC interstitial alloy FeC at zero pressure [7], the nonlinear deformation of BCC metal Fe and BCC interstitial alloy FeSi [8], jumps of volume, enthalpy and entropy at the melting point, the thermal conductivity and the thermal diffusivity for FCC-Au [9], the equilibrium vacancy concentration and thermodynamic quantities of BCC defective alloys FeCrSi and VWSi under pressure [10], the melting and the Debye



Citation: Hoa, N.T.; Hoc, N.Q.; Dat, H.X. Study on the Thermodynamic Properties of Thin Film of FCC Interstitial Alloy AuSi at Zero Pressure Using the Statistical Moment Method. *Physics* **2023**, *5*, 59–68. https://doi.org/10.3390/ physics5010005

Received: 10 November 2022 Revised: 21 December 2022 Accepted: 22 December 2022 Published: 6 January 2023



Copyright: © 2023 by the authors. Licensee MDPI, Basel, Switzerland. This article is an open access article distributed under the terms and conditions of the Creative Commons Attribution (CC BY) license (https:// creativecommons.org/licenses/by/ 4.0/). temperature for BCC and FCC metals under pressure [11], the elastic deformation and the velocity of elastic wave for metal Fe and its BCC interstitial alloys [12], the Young modulus and the stress-strain curve for Fe and FeC [13] and melting behaviors of hcp iron up to 4000 GPa [14]. The SMM has still been applied to study the thermodynamic properties of metal thin films [15,16]. The average values of the Young's moduli are 63 GPa for Ag and 57 GPa for Al multilayers [16]. The thermomechanical properties of gold (Ag), silver (Au) and aluminum (Al) thin films have attracted the attention of researchers recently [17,18]. The mechanical stresses and the coefficients of linear thermal expansion were investigated by using non-ambient (in-situ) X-ray diffraction measurements [19]. A novel theory was developed to predict the growth mode of a thin metallic film on an insulating substrate [20]. To further investigate nanoindentation data of film-substrate systems and to learn more about the mechanical properties of nanometer film-substrate systems, two kinds of films on different substrate systems have been tested with a systematic variation in film thickness and substrate characteristics [21]. The coefficient of thermal expansion, biaxial modulus and stress of some metallic (Ag and Al) thin films were measured using the thermally induced bending technique [22]. The Young's modulus of free-standing polycrystalline Al and Au films with submicron thickness has been studied using a dynamic bulge-testing technique [23]. Melting temperatures of refractory metals are studied at high pressures [24].

The size-dependences of the melting point, Debye temperature, thermal expansion coefficient (TEC) and specific heat of nanostructured materials have been modeled free of adjustable parameters. The melting point and Debye temperature decrease while the thermal expansion coefficient and specific heat increase when the grain size decreases [25]. A new analytical method for temperature- and size-dependent TEC of transition metallic nanostructures has been established [26]. As an important property for reflecting the binding forces between atoms, the Debye temperature of nanocrystals can be tuned according to size, dimensionality and composition. In order to understand how these factors influence the Debye temperature, a new nanothermodynamic model without any adjustable parameters is established here by considering the surface stress and bond number simultaneously. The Debye temperature decreases with a decrease in size if the dimensionality is given, while the size effect on nanowires is stronger than that on thin films and weaker than that on nanoparticles. It is also found that the Debye temperature of nanoalloys decreases with the increase in the component with smaller cohesive energy for the same size and dimensionality. The validity of the model is proved by the good consistency between the model predictions and experimental and computer simulation results [27].

Au and gold silicide (AuSi) have many applications in superconducting wire technology [28]. AuSi is commercially available and used in bearing assembly, ballast, casting, step welding and radiation shielding. In the current study, we modelled a face-centered cubic (FCC) binary interstitial alloy's thin film and developed the thermodynamic theory of this thin film based on the SMM [6–16,29,30]. Here, first, the theoretical results of the Au film are numerically calculated, and are compared with reported calculations and experiments to confirm the precision of the calculation model developed in this paper. Then, the model is applied to the AuSi alloy film to discover new properties caused by the Si concentration.

2. Methods, Results and Discussion

2.1. Model and Calculation Method

Consider a free thin film of FCC interstitial alloy AB. Assume this film has n^* layers with the thickness d. The thin film consists of two outer layers, two next outer layers and n^* -4 inner layers. Let N^{ol} , N^{nol} and N^{il} be the number of atoms in the outer layer, the next outer layer and the inner layer of this thin film, respectively [6].

For the layer *l* (this layer is the inner layer or the next outer layer), the displacement of the atom X (X = A, A_1 , A_2 , B, where A is the atom in the pure metal A, A_1 is the main metal atom A at the body center of the cubic unit cell, A_2 is the main metal atom A at the vertices of the cubic unit cell and B is the interstitial atom at the face center of the cubic unit cell) at pressure P and temperature T from the equilibrium position has the form [6,29]:

$$y_{X}^{l} = \sqrt{\frac{2\gamma_{X}^{l}\theta^{2}}{3(k_{X}^{l})^{3}}A_{X}^{l}}A_{X}^{l} \equiv a_{1X}^{l} + \sum_{i=2}^{6} \left(\frac{\gamma_{X}^{l}\theta}{(k_{X}^{l})^{2}}\right)^{i}a_{iX}^{i},$$

$$a_{1X}^{l} = 1 + \frac{1}{2}Y_{X}^{l},$$

$$a_{2X}^{l} = \frac{13}{3} + \frac{47}{6}Y_{X}^{l} + \frac{23}{6}\left(Y_{X}^{l}\right)^{2} + \frac{1}{2}\left(Y_{X}^{l}\right)^{3},$$

$$a_{3X}^{l} = -\left(\frac{25}{3} + \frac{121}{6}\left(Y_{X}^{l}\right) + \frac{50}{3}\left(Y_{X}^{l}\right)^{2} + \frac{16}{3}\left(Y_{X}^{l}\right)^{3} + \frac{1}{2}\left(Y_{X}^{l}\right)^{4}\right),$$

$$a_{4X}^{l} = \frac{43}{3} + \frac{93}{2}\left(Y_{X}^{l}\right) + \frac{169}{3}\left(Y_{X}^{l}\right)^{2} + \frac{83}{3}\left(Y_{X}^{l}\right)^{3} + \frac{22}{3}\left(Y_{X}^{l}\right)^{4} + \frac{1}{2}\left(Y_{X}^{l}\right)^{5},$$

$$a_{5X}^{l} = -\left(\frac{103}{3} + \frac{749}{6}\left(Y_{X}^{l}\right) + \frac{363}{2}\left(Y_{X}^{l}\right)^{2} + \frac{391}{3}\left(Y_{X}^{l}\right)^{3} + \frac{148}{3}\left(Y_{X}^{l}\right)^{4} + \frac{53}{6}\left(Y_{X}^{l}\right)^{5} + \frac{1}{2}\left(Y_{X}^{l}\right)^{6}\right),$$

$$a_{6X}^{l} = 65 + \frac{561}{2}\left(Y_{X}^{l}\right) + \frac{1489}{3}\left(Y_{X}^{l}\right)^{2} + \frac{927}{2}\left(Y_{X}^{l}\right)^{3} + \frac{145}{2}\left(Y_{X}^{l}\right)^{3} + \frac{145}{2}\left(Y_{X}^{l}\right)^{3} + \frac{145}{2}\left(Y_{X}^{l}\right)^{3}\right),$$

$$(1)$$

where $\theta = k_{Bo}T$, k_{Bo} is the Boltzmann constant, T is the absolute temperature, $y_X^l \equiv y_X^l(P,T)$, k_X^l is the harmonic crystal parameter of the atom X in the layer l and γ_X^l is the anharmonic crystal parameter of the atom X in the layer l. Parameters k_X^l and γ_X^l are determined at pressure P and temperature T = 0 K from the nearest neighbor distance $r_{1X}^l(P,0)$ between two atoms in the layer l, and this distance is calculated using the following equation of state [30]:

$$Pv_X^l = -r_{1X}^l \left(\frac{1}{6} \frac{\partial u_{0X}^l}{\partial r_{1X}^l} + \frac{\hbar \omega_X^l}{4k_X^l} \frac{\partial k_X^l}{\partial r_{1X}^l} \right), \tag{2}$$

where u_{0X}^l is the cohesive energy of the atom *X* in the layer *l*, $v_X^l = \frac{r_{1X}^{l3}}{\sqrt{2}}$ is the volume of the cubic unit cell per atom *X* in the layer *l* for FCC lattices, and $x_X^l = \frac{\hbar \omega_X^l}{2\theta} = \frac{\hbar}{2\theta} \sqrt{\frac{k_X^l}{m_X^l}}$, where m_X^l is the mass of the atom *X* in the layer *l* and \hbar is the Planck's constant. For the outer layer, the displacement of the atom *X* is equal to [6,30]

$$y_X^{\text{ol}} = -\frac{\gamma_X^{\text{ol}}\theta}{\left(k_X^{\text{ol}}\right)^2} Y_X^{\text{ol}}, \quad Y_X^{\text{ol}} \equiv x_X^{\text{ol}} \text{coth} x_X^{\text{ol}}, \tag{3}$$

where k_X^{ol} , γ_X^{ol} , x_X^{ol} are determined in the same way as above [30].

The nearest neighbor distances between two atoms $r_{1X}(P, T)$ in the layer *m* (this layer is the inner layer, the next outer layer or the outer layer) are determined by using the methods described in Refs. [6,30]:

The mean nearest neighbor distance, $\overline{r_{1A}^{ml}(P,T)}$, between two atoms A in the layer *m* of the FCC interstitial alloy AB is determined by using the methods of Refs. [6,30]:

$$\overline{r_{1A}^{ml}(P,T)} = \overline{r_{1A}^{ml}(P,0)} + \overline{y^{ml}(P,T)}, \overline{r_{1A}^{ml}(P,0)} = \left(1 - c_B^{ml}\right) r_{1A}^{ml}(P,0) + c_B^{ml} r'_{1A}^{ml}(P,0),$$

$$\overline{y^{ml}(P,T)} = \sum_X c_X^{ml} y_X^{ml}(P,T),$$
(5)

where $r'_{1A}^{ml}(P,0) = \sqrt{2}r_{1B}^{ml}(P,0)$, $c_A^{ml} = 1 - 15c_B^{ml}$, $c_{A_1}^{ml} = 6c_B^{ml}$, $c_{A_2}^{ml} = 8c_B^{ml}$ for FCC lattices, $c_X^{ml} = \frac{N_X^{ml}}{N^{ml}}$ is the concentration of atoms *X* in the layer *m*, N_X^{ml} is the number of atoms *X* in the layer *m*, and N^{ml} is the number of atoms in the layer *m*.

The Helmholtz free energy for the layer *l* of FCC binary interstitial alloy's thin film approximately has the form [6]:

$$\Psi^{ml} = N^{ml} \left(\sum_{X} c_X^{ml} \Psi_X^{ml} - TS_c^{ml} \right),$$

$$\Psi_X^{ml} = N^{ml} \Psi_X^{ml} \approx U_{0X}^{ml} + 3N^{ml} \theta [x_X^{ml} + \ln(1 - e^{-2x_X^{ml}})] + \frac{3N^{ml}\theta^2}{(k_X^{ml})^2} \left[\gamma_{2X}^{ml} \left(Y_X^{ml} \right)^2 - \frac{2\gamma_{1X}^{ml}}{3} \left(1 + \frac{Y_X^{ml}}{2} \right) \right] + \frac{6N^{ml}\theta^3}{(k_X^{ml})^4} \left[\frac{4}{3} \left(\gamma_{2X}^{ml} \right)^2 \left(1 + \frac{Y_X^{ml}}{2} \right) Y_X^{ml} - 2 \left(\left(\gamma_{1X}^{ml} \right)^2 + 2\gamma_{1X}^{ml} \gamma_{2X}^{ml} \right) \left(1 + \frac{Y_X^{ml}}{2} \right) \left(1 + Y_X^{ml} \right) \right].$$
(6)

In Equation (6), $U_{0X}^{ml} = \frac{N^{ml}}{2} u_{0X}^{ml}$, ψ_X^{ml} is the Helmholtz free energy of an atom X in the layer *m* and S_c^{ml} is the configurational entropy of the alloy in the layer *m*.

At low temperatures, the vibrations of the atoms around the lattice point nodes are harmonic. Then, the Helmholtz free energies for the layer m of the alloy film have the form [6],

$$\Psi^{ml} = N^{ml} \left(\sum_{X} c_X^{ml} \psi_X^{ml} - T S_c^{ml} \right),$$

$$\Psi^{ml}_X = N^{ml} \psi^{ml}_X \approx U_0^{ml} + 3N^{ml} \theta[x_X^{ml} + \ln(1 - e^{-2x_X^{ml}})].$$
(7)

Assume the thin film consists of *N* atoms with n^* layers and the number of atoms per layer is equal to N^{ml} , then $N = n^* N^{ml}$ and [16]

$$n^* = \frac{N}{N^{ml}}.$$
(8)

The number of atoms in the inner layer, the next outer layer and the outer layer of the thin film, respectively, is determined by [16]

$$N^{\rm il} = (n^* - 4)N^{ml} = \left(\frac{N}{N^{ml}} - 4\right)N^{ml} = N - 4N^{ml},\tag{9}$$

$$N^{\text{nol}} = 2N^{ml} = N - (n^* - 2)N^{ml},$$

$$N^{\text{ol}} = 2N^{ml} = N - (n^* - 2)N^{ml}.$$
(10)

The Helmholtz free energy of the thin film is given by [16]

$$\Psi = \Psi^{il} + \Psi^{nol} + \Psi^{ol} - TS_c = N^{il}\psi^{il} + N^{nol}\psi^{nol} + N^{ol}\psi^{ol} - TS_c$$

= $(N - 2N^{nol} - 2N^{ol})\psi^{il} + 2N^{nol}\psi^{nol} + 2N^{ol}\psi^{ol} - TS_c,$ (11)

where $N = N^{il} + N^{nol} + N^{ol}$ is the total atomic number of the film, S_c is the configurational entropy of the film and ψ^{il} , ψ^{nol} , ψ^{ol} are the Helmholtz free energies of an atom in the inner layer, the next outer layer and the outer layer of the film, respectively.

Let symbol \overline{a} denotes the mean nearest neighbor distance between two atoms, *b* the average thickness of the two respective layers, and \overline{a}_c the average lattice constant of the thin film.

Then, for FCC thin films [16]:

$$\overline{b} = \frac{\overline{a}}{\sqrt{2}}, \ \overline{a}_c = 2\overline{b} = \sqrt{2}\overline{a}.$$
(12)

The thickness is related to the number of layers [16]:

$$d = 2b^{\text{ol}} + 2b^{\text{nol}} + (n^* - 5)b^{\text{il}} = (n^* - 1)\overline{b} = (n^* - 1)\frac{\overline{a}}{\sqrt{2}}$$
(13)

and

$$n^* = 1 + \frac{d}{\overline{b}} = 1 + \frac{d\sqrt{2}}{\overline{a}}.$$
 (14)

The isothermal compressibility and elastic modulus of the FCC interstitial alloy AB's thin film are [6,16,29], respectively:

$$\chi_{TAB} = \frac{3\left(\frac{\bar{a}}{\bar{a}_{0}}\right)^{3}}{2P + \frac{\bar{a}^{2}}{3V} \left(\frac{d\sqrt{2} - 3\bar{a}}{d\sqrt{2} + \bar{a}} \frac{\partial^{2}\Psi_{il}}{\partial a_{il}^{2}} + \frac{2\bar{a}}{d\sqrt{2} + \bar{a}} \frac{\partial^{2}\Psi_{ol}}{\partial a_{ol}^{2}} + \frac{2\bar{a}}{d\sqrt{2} + \bar{a}} \frac{\partial^{2}\Psi_{nol}}{\partial a_{nol}^{2}}\right)_{T}}, B_{TAB} = \frac{1}{\chi_{TAB}}, \quad (15)$$

$$\left(\frac{\partial^2 \psi_{ml}}{\partial a_{ml}^2}\right)_T = \frac{1}{N_{ml}} \sum_X c_X \left(\frac{\partial^2 \Psi_X^{ml}}{\partial a_X^{ml2}}\right)_T = \frac{1}{N_{ml}} \sum_X c_X 3N_X^{ml} \left\{\frac{1}{6} \frac{\partial^2 u_{0X}^{ml}}{\partial a_X^{ml2}} + \frac{\hbar \omega_X^{ml}}{4k_X^{ml}} \left[\frac{\partial^2 k_X^{ml}}{\partial a_X^{ml2}} - \frac{1}{2k_X^{ml}} \left(\frac{\partial k_X^{ml}}{\partial a_X^{ml}}\right)^2\right]\right\}.$$

The thermal expansion coefficient of the FCC interstitial alloy AB's thin film has the form as reported in Refs. [6,16,29]:

$$\alpha_{TAB} = \frac{k_{\rm Bo}}{\bar{a}_0} \frac{d\bar{a}}{d\theta} = \frac{d_{\rm ol}\alpha_{Tol} + d_{\rm nol}\alpha_{Tnol} + (d - d_{\rm ol} - d_{\rm nol})\alpha_{Til}}{d},\tag{16}$$

$$\alpha_{Tml} = \frac{k_{\text{Bo}}}{a_0^{ml}} \frac{\partial y^{ml}(T)}{\partial \theta}, \ \frac{\partial y^{ml}(T)}{\partial \theta} = \sum_X c_X \frac{\partial y^{ml}_X(T)}{\partial \theta} = \sum_X c_X \frac{\partial}{\partial \theta} \sqrt{\frac{2\gamma_X^{ml}(0)\theta^2}{3(k_X^{ml})^3}} A_X^{ml}(T).$$

Here d_{ol} is the thickness of the outer layers, d_{nol} is the thickness of the next outer layers and d is the thickness of a thin film.

The energy of the FCC interstitial alloy AB's thin film reads [6,16,29]:

$$E_{AB} = \Psi_{AB} - \theta \frac{\partial \Psi_{AB}}{\partial \theta} = \frac{d\sqrt{2} - 3\bar{a}}{d\sqrt{2} + \bar{a}} E_{il} + \frac{2\bar{a}}{d\sqrt{2} + \bar{a}} E_{ol} + \frac{2\bar{a}}{d\sqrt{2} + \bar{a}} E_{nol},$$

$$E_{ml} = \sum_{X} c_X E_X^{ml},$$
(17)

$$\begin{split} E_X^{\rm il} &= U_{0X}^{\rm il} + 3\theta N_X^{\rm il} Y_X^{\rm il} + \frac{3\theta^2 N_X^{\rm il}}{k_X^{\rm il2}} \left[\gamma_{2X}^{\rm il} Y_X^{\rm il2} + \frac{\gamma_{1X}^{\rm il}}{3} \left(2 + Z_X^{\rm il2} \right) - 2\gamma_{2X}^{\rm il} Y_X^{\rm il} Z_X^{\rm il2} \right], \\ E_X^{\rm nol} &= U_{0X}^{\rm nol} + 3\theta N_X^{\rm nol} Y_X^{\rm nol} + \frac{3\theta^2 N_X^{\rm nol}}{k_X^{\rm nol2}} \left[\gamma_{2X}^{\rm nol} Y_X^{\rm nol2} + \frac{\gamma_{1X}^{\rm nol}}{3} \left(2 + Z_X^{\rm nol2} \right) - 2\gamma_{2X}^{\rm nol} Y_X^{\rm nol} Z_X^{\rm nol2} \right], \\ E_X^{\rm nol} &= U_{0X}^{\rm ol} + 3\theta N_X^{\rm ol} Y_X^{\rm nol} + \frac{3\theta^2 N_X^{\rm nol}}{k_X^{\rm nol2}} \left[\gamma_{2X}^{\rm nol} Y_X^{\rm nol2} + \frac{\gamma_{1X}^{\rm nol}}{3} \left(2 + Z_X^{\rm nol2} \right) - 2\gamma_{2X}^{\rm nol} Y_X^{\rm nol} Z_X^{\rm nol2} \right], \\ E_X^{\rm old} &= U_{0X}^{\rm old} + 3\theta N_X^{\rm ol} Y_X^{\rm ol}. \end{split}$$

The specific heat at constant volume of the FCC interstitial alloy AB's thin film has the following form [6,16,29]:

$$C_{VAB} = \frac{d\sqrt{2} - 3\bar{a}}{d\sqrt{2} + \bar{a}} C_{V}^{\text{il}} + \frac{2\bar{a}}{d\sqrt{2} + \bar{a}} C_{V}^{\text{ol}} + \frac{2\bar{a}}{d\sqrt{2} + \bar{a}} C_{V}^{\text{nol}},$$
(18)

$$C_{V}^{ml} = \sum_{X} c_{X} C_{VX}^{ml},$$

$$C_{VX}^{il} = 3k_{\text{Bo}} N_{X}^{\text{il}} \Big\{ Z_{X}^{\text{il}2} + \frac{2\theta}{k_{X}^{\text{il}2}} \Big[\Big(2\gamma_{2X}^{\text{il}} + \frac{\gamma_{1X}^{\text{il}}}{3} \Big) Y_{X}^{\text{il}} Z_{X}^{\text{il}2} + \frac{\gamma_{1X}^{\text{il}}}{3} \Big(1 + Z_{X}^{\text{il}2} \Big) - \gamma_{2X}^{\text{il}} \Big(Z_{X}^{\text{il}4} + Y_{X}^{\text{il}2} Z_{X}^{\text{il}2} \Big) \Big] \Big\},$$

$$(18)$$

$$C_{VX}^{\text{nol}} = 3k_{\text{Bo}}N_X^{\text{nol}} \Big\{ Z_X^{\text{nol}2} + \frac{2\theta}{k_X^{\text{nol}2}} \left[\left(2\gamma_{2X}^{\text{nol}} + \frac{\gamma_{1X}^{\text{nol}}}{3} \right) Y_X^{\text{nol}} Z_X^{\text{nol}2} + \frac{\gamma_{1X}^{\text{nol}}}{3} \left(1 + Z_X^{\text{nol}2} \right) - \gamma_{2X}^{\text{nol}} \left(Z_X^{\text{nol}4} + Y_X^{\text{nol}2} Z_X^{\text{nol}2} \right) \right] \Big\},$$
$$C_{VX}^{\text{ol}} = 3k_{\text{Bo}} N_X^{\text{ol}} Z_X^{\text{ol}2}.$$

In Equations (17) and (18), $Z_X^{ml} \equiv \frac{x_X^{ml}}{\sinh x_X^{ml}}$. The specific heat at constant pressure of the FCC interstitial alloy AB's thin film reads [6,16,29]:

$$C_{PAB} = C_{VAB} + \frac{9TV_{AB}\alpha_{TAB}^2}{\chi_{TAB}}.$$
(19)

2.2. Numerical Results and Discussion for Alloy AuSi

For evaluating the interaction of Au-Au and Si-Si in the alloy AuSi, the Mie-Lennard-Jones potential [31],

$$p(r) = \frac{D}{n-m} \left[m \left(\frac{r_0}{r}\right)^n - n \left(\frac{r_0}{r}\right)^m \right],\tag{20}$$

was used, where *D* is the depth of the potential well corresponding to the equilibrium distance r_0 , while *m* and *n* are determined empirically. The obtained parameters *D*, r_0 , *m*, *n* are given in Table 1. Considering the interactions for Au-Si, the following approximation was used:

$$\varphi_{\mathrm{Au-Si}} \approx \frac{1}{2}(\varphi_{\mathrm{Au-Au}} + \varphi_{\mathrm{Si-Si}}).$$
 (21)

Table 1. The parameters *D*, *r*₀, *m*, *n* [32] for the Mie-Lennard-Jones potential (20).

Interaction	т	п	D (10 ^{−16} erg)	<i>r</i> ₀ (10 ^{−10} m)		
Au-Au [33]	1.96	15.56	10,227.78	2.8751		
Si-Si [28]	6.0	12.0	45,128.24	2.295		

The influence of temperature and layer number on the nearest neighbor distance, *a*, isothermal elastic modulus, B_T , thermal expansion coefficient, α_T , specific heat at constant volume, C_{V_i} and specific heat at constant pressure, C_P , for Au at P = 0 were calculated using the SMM, and the reported calculations [33–37] are given in Table 2.

According to Table 2, the SMM calculations for isothermal elastic modulus, thermal expansion coefficient, specific heat at constant volume and specific heat at constant pressure of Au at P = 0 in the range of temperature from 100 to 800 K are in good agreement with the data of reported experiments [38] and calculations [33–37]. When the number of layers increases, the thickness of the film, the mean nearest neighbor distance, the thermal expansion coefficient and the specific heats at constant volume and at constant pressure increase, while the isothermal elastic modulus decreases. The obtained SMM calculations are consistent with the results obtained in Ref. [25], wherein the nanoparticle size increases with the decrease in the coefficient of thermal expansion and specific heat. When the nanoparticle size changes, the cohesive energy and the mean nearest neighbor distance change, and therefore, the thermal expansion coefficient and the specific nearest neighbor distance. This is consistent with the results from Ref. [26].

The influence of silicon concentration, temperature and layer number on the mean nearest neighbor distance, *a*, isothermal elastic modulus, B_T , thermal expansion coefficient, α_T , specific heat at constant volume, C_V , and specific heat at constant pressure, C_P , for AuSi at P = 0 were calculated using the SMM and are given in Table 3.

According to Tables 2 and 3, the nearest neighbor distance of the thin film depends strongly on the thickness and temperature. The nearest neighbor distance of the thin film increases as the film becomes thicker and increases sharply as the temperature rises. The temperature-dependence of the nearest neighbor distance is because the atoms vibrate more strongly and the nearest neighbor distance increases when the temperature increases.

As the temperature increases, the kinetic energy of the atoms increases and the anharmonicity of lattice vibrations is larger, making the mean nearest neighbor distance between two atoms in the alloy, the thermal expansion coefficient, the specific heat at constant volume and the specific heat at constant pressure increase while the isothermal elastic modulus decreases. As the interstitial atom concentration increases, the lattice expands, the mean nearest neighbor distance between two atoms in the alloy, the thermal expansion coefficient, the specific heat at constant volume and the specific heat at constant pressure increase while the isothermal elastic modulus decreases. As the number of layers increases until about 100 layers (about 35 nm thickness), the thermal expansion coefficient, the specific heat at constant volume, the specific heat at constant pressure and the isothermal elastic modulus of the thin film approach the values of the bulk material.

Table 2. Dependence of the nearest neighbor distance, \bar{a} , isothermal elastic modulus, B_T , thermal expansion coefficient, α_T , specific heat at constant volume, C_V , and specific heat at constant pressure, C_P , for Au at P = 0 on the temperature, T, and number of layers calculated here using the statistical moments method (SMM) and compared with the corresponding values calculated (CAL) from Refs. [33–37] and the experimental (EXPT) data [38].

		T (K)								
Quantity	Number of Layers		100	200	300	400	500	600	700	800
		10	3.146	3.152	3.159	3.166	3.173	3.180	3.189	3.197
		15	3.033	3.039	3.045	3.052	3.058	3.065	3.073	3.080
$-\left(\circ \right)$		30	2.929	2.934	2.940	2.946	2.952	2.958	2.965	2.972
$\overline{a} \begin{pmatrix} \circ \\ A \end{pmatrix}$		50	2.889	2.894	2.900	2.905	2.911	2.917	2.924	2.930
		100	2.860	2.865	2.870	2.876	2.881	2.887	2.894	2.900
		Bulk	2.834	2.839	2.844	2.847	2.855	2.861	2.867	2.873
		10	1.334	1.270	1.207	1.145	1.084	1.024	0.963	0.902
		15	1.419	1.353	1.288	1.224	1.161	1.099	1.037	0.975
B_T		30	1.506	1.438	1.371	1.306	1.241	1.178	1.115	1.052
$(10^{11} Pa^{-1})$		50	1.541	1.473	1.405	1.339	1.274	1.210	1.146	1.083
		100	1.568	1.499	1.431	1.365	1.299	1.234	1.171	1.107
		Bulk	1.593	1.523	1.455	1.388	1.322	1.257	1.192	1.129
	CAL [33]	Bulk	1.710	1.666	1.623	1.586	1.549	1.515	1.485	1.458
	CAL [34]	Bulk	1.696	1.658	1.612	1.575	1.526	-	-	-
		10	1.557	1.797	1.913	2.015	2.120	2.235	2.365	2.521
		15	1.515	1.749	1.859	1.955	2.052	2.157	2.275	2.411
α_T		30	1.474	1.702	1.806	1.895	1.984	2.079	2.184	2.301
$\begin{pmatrix} \alpha_T \\ (10^{-5} \mathrm{K}^{-1}) \end{pmatrix}$		50	1.457	1.682	1.784	1.871	1.957	2.048	2.147	2.257
		100	1.445	1.668	1.768	1.852	1.936	2.025	2.120	2.224
		Bulk	1.433	1.655	1.754	1.836	1.918	2.004	2.095	2.195
	CAL [37]	Bulk	1.442	1.636	1.696	1.774	1.854	1.915	1.975	2.036
	CAL [34]	Bulk	1.270	1.428	1.536	1.655	1.773	1.940	2.137	2.423
	CAL [35]	Bulk	1.359	1.704	1.842	-	-	-	-	-
	EXPT [38]	Bulk	1.15	1.34	1.41	1.45	1.50	1.54	1.59	1.65
		10	5.231	5.797	5.919	5.972	6.007	6.035	6.061	6.089
		15	5.217	5.793	5.916	5.969	6.003	6.031	6.056	6.082
C_V		30	5.202	5.788	5.913	5.966	6.000	6.027	6.051	6.075
$(cal/(mol \cdot K))$		50	5.196	5.786	5.912	5.965	5.999	6.025	6.049	6.072
		100	5.191	5.784	5.911	5.964	5.998	6.024	6.047	6.070
		Bulk	5.187	5.783	5.910	5.964	5.997	6.023	6.046	6.068
		10	5.324	6.033	6.302	6.513	6.721	6.940	7.183	7.464
		15	5.300	6.006	6.262	6.457	8.115	6.842	7.056	7.298
$\binom{C_P}{(\text{cal}/(\text{mol}\cdot\text{K}))}$		30	5.277	5.981	6.226	6.406	6.576	6.752	6.940	7.148
		50	5.268	5.971	6.212	6.387	6.551	6.719	6.897	7.092
		100	5.262	5.964	6.202	6.373	6.532	6.694	6.866	7.051
		Bulk	5.256	5.958	6.193	6.361	6.516	6.673	6.838	7.015
	CAL [33]	Bulk	5.542	5.994	6.112	6.277	6.371	6.464	6.558	6.604
	CAL [36]	Bulk	5.136	5.875	5.873	6.301	6.419	6.560	6.677	6.771
	EXPT [38]	Bulk	5.12	5.84	6.07	6.18	6.28	6.40	6.52	6.65

Quantity		T (K)	100	300	500	800	100	300	500	800	
2	Number of Layers		c _{Si} = 1%				c _{Si} = 3%				
$\overline{a}_{AB} \left(\stackrel{\mathrm{o}}{\mathrm{A}} \right)$	10		3.153	3.165	3.178	3.200	3.168	3.178	3.189	3.206	
	15		3.041	3.052	3.064	3.084	3.055	3.064	3.074	3.090	
	30		2.936	2.946	2.957	2.975	2.950	2.958	2.967	2.982	
	50		2.896	2.906	2.916	2.934	2.909	2.918	2.926	2.940	
	100		2.866	2.876	2.887	2.903	2.880	2.888	2.897	2.910	
	Bulk		2.841	2.850	2.860	2.877	2.854	2.862	2.870	2.884	
$\begin{array}{c} B_{TAB} \\ \left(10^{11} \mathrm{Pa}^{-1}\right) \end{array}$	10		2.373	2.198	2.028	1.776	4.439	4.178	3.923	3.545	
	15		2.521	2.340	2.165	1.906	4.713	4.442	4.177	3.787	
	30		2.673	2.487	2.306	2.041	4.995	4.714	4.439	4.037	
	50		2.736	2.547	2.363	2.096	5.110	4.825	4.546	4.139	
()	100		2.783	2.592	2.407	2.138	5.198	4.909	4.628	4.217	
	Bulk		2.826	2.633	2.447	2.176	5.277	4.986	4.702	4.288	
$\begin{pmatrix} \alpha_{TAB} \\ \left(10^{-5} \mathrm{K}^{-1} \right) \end{pmatrix}$	10		0.821	1.048	1.139	1.280	0.382	0.552	0.600	0.658	
	15		0.800	1.022	1.108	1.239	0.373	0.539	0.585	0.641	
	30		0.779	0.996	1.077	1.197	0.363	0.526	0.571	0.623	
	50		0.770	0.985	1.065	1.181	0.359	0.521	0.565	0.616	
	100		0.764	0.977	1.056	1.169	0.356	0.517	0.561	0.611	
	Bulk		0.758	0.970	1.048	1.157	0.354	0.514	0.557	0.606	
C_{VAB} (cal/(mol·K))	10		4.886	5.849	5.975	6.064	4.195	5.709	5.910	6.015	
	15		4.870	5.845	5.971	6.058	4.177	5.704	5.907	6.011	
	30		4.854	5.841	5.968	6.052	4.158	5.699	5.904	6.006	
			4.848	5.840	5.967	6.050	4.151	5.696	5.902	6.004	
	100		4.843	5.839	5.966	6.048	4.146	5.695	5.901	6.003	
	Bulk		4.838	5.838	5.965	6.046	4.141	5.693	5.900	6.002	
C _{PAB} (cal/(mol·K))	10		4.932	6.060	6.362	6.764	4.214	5.822	6.120	6.387	
	15		4.912	6.037	6.322	6.687	4.194	5.806	6.098	6.347	
	30		4.892	6.015	6.285	6.617	4.174	5.792	6.077	6.311	
			4.884	6.007	6.272	6.591	4.166	5.786	6.069	6.298	
	100		4.878	6.001	6.262	6.572	4.160	5.782	6.064	6.288	
	Bulk		4.873	5.996	6.253	6.555	4.155	5.778	6.059	6.279	

Table 3. Dependence of the mean nearest neighbor distance, \bar{a} , isothermal elastic modulus, B_T , thermal expansion coefficient, α_T , specific heat at constant volume, C_V , and specific heat at constant pressure, C_P , on the silicon concentration, c_{Si} , temperature, T, and number of layers for AuSi at P = 0 calculated using the SMM.

For bulk Au at the near melting temperature, the atomic volumes calculated using the SMM in the current study and that in a reported study are 17.29×10^{-30} m³ and 17.88×10^{-30} m³ [39], respectively. Clearly, these calculations are consistent, confirming the reliability of our calculation. For bulk Au at T = 300 K and P = 0, the nearest neighbor distance calculated using the SMM in the current study is 2.8454×10^{-10} m, and this result is in good agreement with the experimental data (2.8838×10^{-10} m) reported in Ref. [40].

3. Conclusions

Based on the model and the thermodynamic theory for FCC binary interstitial alloy's thin films built using the SMM, we performed numerical calculations for AuSi films in the temperature range from 100 to 800 K, considering the variation of interstitial atom concentration from zero to 3% and the change of number of layers from 10 to 200. When the interstitial atom concentration is zero, the thermodynamic quantities of the interstitial alloy's thin film become those of the main-metal thin film. The thermal expansion coefficient, the specific heat at constant volume and the specific heat at constant pressure increase while the isothermal elastic modulus decreases with increasing temperature and increasing interstitial atom concentration. As the number of layers increases up to 100 layers (about 35 nm thickness), thermodynamic quantities of the thin film approach those values of

the bulk material. The SMM calculations of the nearest neighbor distance, the thermal expansion coefficient, the specific heat at constant volume and the specific heat at constant pressure for Au in the form of bulk materials are in good agreement with the results of reported experiments and calculations. The obtained numerical results without comparative data are new and represent a useful reference for designing future experiments.

Author Contributions: conceptualization, N.T.H.; methodology, N.Q.H.; validation, H.X.D.; investigation, H.X.D.; data curation, N.Q.H.; writing—original draft, N.T.H.; writing—review & editing, N.Q.H. and H.X.D.; supervision, N.T.H.; funding acquisition, N.T.H. All authors have read and agreed to the published version of the manuscript.

Funding: This research is funded by University of Transport and Communications (UTC) under grant number T2022-CB-010.

Data Availability Statement: Not applicable.

Conflicts of Interest: The authors declare no conflict of interest.

References

- 1. Nazarov, A.A.; Bachurin, D.V.; Ni, Z.L. Atomistic simulation of ultrasonic welding of copper. Metals 2022, 12, 2033. [CrossRef]
- Yu, Y.-X. Effect of defects and solvents on silicene cathode of nonaqueous lithium–oxygen batteries: A theoretical investigation. *J. Phys. Chem. C* 2019, 123, 205–213. [CrossRef]
- Malinowska-Adamska, C. Thermodynamic and transport properties of crystals in anharmonic approximation. *Phys. Stat. Sol. B* 1981, 106, 359–367. [CrossRef]
- Karasevskii, A.I.; Lubashenko, V.V. Calculation of thermodynamic properties of Cu and Ag using a self-consistent statistical method. *Phys. Stat. Sol. B* 2004, 241, 1274–1280. [CrossRef]
- 5. Tang, N.; Hung, V.V. Investigation of the thermodynamic properties of anharmonic crystals by the momentum method, I. General results for face-centered cubic crystals. *Phys. Stat. Sol. B* **1988**, *149*, 511–519. [CrossRef]
- 6. Hoc, N.Q.; Tinh, B.D.; Hien, N.D. Elastic moduli and elastic constants of interstitial alloy AuCuSi with FCC structure under pressure. *High Temp. Mater. Proc.* 2019, *38*, 264–272. [CrossRef]
- Tinh, B.D.; Hoc, D.Q.; Vinh, D.Q.; Cuong, T.D.; Hien, N.D. Thermodynamic and elastic properties of interstitial alloy FeC with BCC structure at zero pressure. *Adv. Mater. Sci. Eng.* 2018, 2018, 5251741. [CrossRef]
- 8. Hoc, N.Q.; Tinh, B.D.; Hien, N.D.; Gelu, C.G. Nonlinear deformation of BCC metal Fe and BCC interstitial alloy FeSi: Dependence on temperature, pressure and silicon concentration. *Mater. Phys. Mech.* **2021**, *47*, 501–513. [CrossRef]
- Hoc, N.Q.; Tinh, B.D.; Hien, N.D.; Viet, L.H. On the jumps of volume, enthalpy and entropy at the melting point, the thermal conductivity and the thermal diffusivity for Au with FCC structure: Temperature and pressure dependences. *Prog. Phys. Metals* 2021, 22, 511–530. [CrossRef]
- 10. Hoc, N.Q.; Viet, L.H.; Dat, H.X. Equilibrium vacancy concentration and thermodynamic quantities of BCC defective alloys FeCrSi and VWSi under pressure. *Mod. Phys. Lett. B* 2022, *36*, 2250105. [CrossRef]
- 11. Hoc, N.Q.; Tinh, B.D.; Hien, N.D. The melting and the Debye temperature for BCC and FCC metals under pressure: A calculation from the statistical moment method. *Arch. Metallur. Mater.* **2022**, *67*, 1227–1234. [CrossRef]
- Hoc, N.Q.; Hien, N.D.; Vi, T.K. Elastic deformation and velocity of elastic wave for metal Fe and its interstitial alloys with BCC structure: Dependence on temperature, pressure and concentration of interstitial atoms. *Phys. B* 2022, 644, 414134. [CrossRef]
- 13. Hoc, N.Q.; Dung, N.T.; Cuong, N.C.; Tinh, B.D.; Hien, N.D.; Van, C.L.; Umut, S.; Stefan, T. Determination of the Young modulus and the stress-strain curve for Fe and binary FeC interstitial alloy. *J. Compos. Sci.* **2022**, *6*, 250. [CrossRef]
- 14. Cuong, T.D.; Hoc, N.Q.; Trung, N.D.; Thao, N.T.; Anh, D.P. Theoretical predictions about melting behaviors of hcp iron up to 4000 GPa. *Phys. Rev. B* 2022, *106*, 094103. [CrossRef]
- 15. Hung, V.V.; Phuong, D.D.; Hoa, N.T.; Hieu, H.K. Theoretical investigation of thermodynamic properties of metallic thin films. *Thin Sol. Films* **2015**, *583*, 7–12. [CrossRef]
- 16. Hung, V.V.; Phuong, D.D.; Hoa, N.T. Investigation of thermodynamic properties of metal thin film by statistical moment method. *Comm. Phys.* **2013**, *23*, 301–311. [CrossRef]
- 17. Haibo, H.; Spaepen, F. Tensilie testing of free-standing Cu, Ag and Al thin films and Ag/Cu multilayers. *Acta Mater.* **2000**, *48*, 3261–3269. [CrossRef]
- Vaz, A.R.; Salvadori, M.C.; Cattani, M. Young modulus measurement of nanostructured metallic thin films. J. Metast. Nanocrystal. Mater. 2004, 20–21, 758–762.
- 19. Kuru, Y.; Wohlschlogel, M.; Welzel, U.; Mittemeijer, E.J. Coefficients of thermal expansion of thin metal films investigated by non-ambient X-ray diffraction stress analysis. *Surf. Coat. Technol.* **2008**, *202*, 2306–2309. [CrossRef]
- 20. Fuks, D.; Dorfman, S.; Zhukovskii, Y.F.; Kotomin, E.A.; Stoneham, A.M. Theory of the growth mode for a thin metallic film on an insulating substrate. *Surf. Sci.* 2002, 499, 24–40. [CrossRef]

- Chen, S.; Liu, L.; Wang, T. Investigation of the mechanical properties of thin films by nanoindentation considering the effects of thickness and different coating-substrate combinations. *Surf. Coat. Technol.* 2005, 191, 25–32. [CrossRef]
- 22. De Lima, M.M.; Lacerda, R.G.; Vilcarromero, J.; Marques, F.C. Coefficient of thermal expansion and elastic modulus of thin films. *J. Appl. Phys.* **1999**, *86*, 4936–4942. [CrossRef]
- Kalkman, A.J.; Verbruggen, A.H.; Janssen, G.C.A.M. Young modulus measurements and grain boundary sliding in free standing thin metal films. *Appl. Phys. Lett.* 2001, 78, 2673–2675. [CrossRef]
- Vereshchagin, L.F.; Fateeva, N.S. Melting temperatures of refractory metals at high pressures. *High Temp. High Pres.* 1977, 9, 619–628. Available online: http://www.oldcitypublishing.com/journals/hthp-electronic-archive-home/hthp-electronic-archive-issue-contents/hthp-volume-9-number-6-1977/ (accessed on 20 December 2022).
- 25. Zhu, Y.F.; Lian, J.S.; Jiang, Q. Modeling of melting point, Debye temperature, thermal expansion coefficient and the specific heat of nanostructured materials. J. Phys. Chem. C 2009, 113, 16896–16900. [CrossRef]
- Zhu, M.; Liu, J.; Huang, Q.; Dong, J.; Yang, X. Temperature and size modulation of the lattice thermal expansion on transition metallic nanostructures. J. Phys. D Appl. Phys. 2022, 55, 485303. [CrossRef]
- 27. Ma, Y.-L.; Zhu, K.; Li, M. Size, dimensionality and composition effects on the Debye temperature of nanocrystals. *Phys. Chem. Chem. Phys.* **2018**, *20*, 27539–27544. [CrossRef]
- Nyilas, R.D.; Frank, S.; Spolenak, R. Revealing plastic deformation mechanisms in polycrystalline thin films with synchrotron XRD. JOM (J. Miner. Metals Mater. Soc.) 2010, 62, 44–51. [CrossRef]
- 29. Tang, N.; Hung, V.V. Investigation of the thermodynamic properties of anharmonic crystals by the momentum method. II. Comparison of calculations with experiments for inert gas crystals. *Phys. Stat. Sol. B* **1990**, *161*, 165–171. [CrossRef]
- 30. Tang, N.; Hung, V.V. Investigation of the thermodynamic properties of anharmonic crystals by the momentum method. III. Thermodynamic properties of the crystals at various pressures. *Phys. Stat. Sol. B* **1990**, *162*, 371–377. [CrossRef]
- 31. Magomedov, M.N. On calculating the Debye temperature and the Gruneisen parameter. *Russ. J. Phys. Chem. A* [*Zh. Fiz. Khim.*] **1987**, *61*, 1003–1009. (In Russian)
- 32. Magomedov, M.N. The calculation of the parameters of the Mie–Lennard-Jones potential. High Temp. 2006, 44, 513–529. [CrossRef]
- Jin, H.-S.; Song, P.; Jon, C.-G.; Kim, J.-C. Thermodynamic properties of FCC metals using reparameterized MEAM potentials. *Ind. J. Phys.* 2021, 95, 2553–2565. [CrossRef]
- 34. Bian, Q.; Bose, S.K.; Shukla, R.C. Vibrational and thermodynamic properties of metals from a model embedded-atom potential. *J. Phys. Chem. Sol.* **2008**, *69*, 168–181. [CrossRef]
- 35. Pandya, C.V.; Vyas, P.R.; Pandya, T.C.; Gohel, V.B. Volume variation of Gruneisen parameters of FCC transition metals. *Bull. Mater. Sci.* 2002, 25, 63–67. [CrossRef]
- Balluffi, W. Vacancy defect mobilities and binding energies obtained from annealing studies. J. Nucl. Mater. 1978, 69–70, 240–263. [CrossRef]
- Grabowski, B.; Hickel, T.; Neugebauer, J. Ab initio study of the thermodynamic properties of nonmagnetic elementary FCC metals: Exchange-correlation-related error bars and chemical trends. *Phys. Rev. B* 2007, *76*, 024309. [CrossRef]
- Gray, D.E. (Ed.) American Institute of Physics Handbook; McGraw-Hill Book Company, Inc.: New York, NY, USA, 1961; Available online: https://www.scribd.com/doc/156529345/American-Institute-of-Physics-Handbook (accessed on 20 December 2022).
- Burakovsky, L.; Greeff, C.W.; Preston, D.L. Analytic model of the shear modulus at all temperatures and densities. *Phys. Rev. B* 2003, 67, 094107. [CrossRef]
- Lide, D.R. (Ed.) CRC Handbook of Chemistry and Physics; CRC Press/Taylor & Francis Group: Boca Raton, FL, USA, 2005; Available online: http://webdelprofesor.ula.ve/ciencias/isolda/libros/handbook.pdf (accessed on 20 December 2022).

Disclaimer/Publisher's Note: The statements, opinions and data contained in all publications are solely those of the individual author(s) and contributor(s) and not of MDPI and/or the editor(s). MDPI and/or the editor(s) disclaim responsibility for any injury to people or property resulting from any ideas, methods, instructions or products referred to in the content.